JACS
JOURNAL OF THE AMERICAN CHEMICAL SOCIETY
Article
pubs.acs.org/JACS

Tuning Magnetism of $[MnSb_4]^{9-}$ Cluster in $Yb_{14}MnSb_{11}$ through Chemical Substitutions on Yb Sites: Appearance and Disappearance of Spin Reorientation

Yufei Hu,[†] Chih-Wei Chen,[‡] Huibo Cao,[§] F. Makhmudov,[∥] Jason H. Grebenkemper,[†] M. N. Abdusalyamova,[∥] Emilia Morosan,[‡] and Susan M. Kauzlarich*[,†]

[†]Department of Chemistry, University of California, One Shields Avenue, Davis, California 95616, United States
[‡]Department of Physics and Astronomy, Rice University, 6100 Main Street, Houston, Texas 77005, United States
[§]Quantum Condensed Matter Division, Oak Ridge National Laboratory, Oak Ridge, Tennessee 37831, United States
[∥]Institute of Chemistry of Tajik Academy of Sciences, 299/2 Ajni Street, Dushanbe 734063, Tajikistan

Supporting Information

ABSTRACT: Single crystals of $Yb_{14-x}RE_xMnSb_{11}$ ($0 < x < 0.6$, *RE* = Pr, Nd, Sm, and Gd) were synthesized by Sn flux. The compounds are iso-structural with $Ca_{14}AlSb_{11}$ ($I4_1/acd$), and their compositions were determined by wavelength-dispersive spectroscopy. $Yb_{14}MnSb_{11}$ is described as a partially screened d-metal Kondo system with the isolated $[MnSb_4]^{9-}$ tetrahedral cluster having a d^5 + hole configuration that results in four unpaired electrons measured in the ferromagnetically ordered phase. All of the Yb atoms in $Yb_{14}MnSb_{11}$ are present as Yb^{2+}, and the additional *RE* in $Yb_{14-x}RE_xMnSb_{11}$ is trivalent, contributing one additional electron to the structure and altering the magnetic properties. All compounds show ferromagnetic ordering in the range of 39−52 K attributed to the $[MnSb_4]^{9-}$ magnetic moment. Temperature-dependent DC magnetization measurements of $Yb_{14-x}Pr_xMnSb_{11}$ ($0.44 \leq x \leq 0.56$) show a sharp downturn right below the ferromagnetic transition temperature. Single-crystal neutron diffraction shows that this downturn is caused by a spin reorientation of the $[MnSb_4]^{9-}$ magnetic moments from the *ab*-plane to *c*-axis. The spin reorientation behavior, caused by large anisotropy, is also observed for similar *x* values of *RE* = Nd but not for *RE* = Sm or Gd at any value of *x*. In Pr-, Nd-, and Sm-substituted crystals, the saturation moments are consistent with ∼4 unpaired electrons attributed to $[MnSb_4]^{9-}$, indicating that local moments of Pr, Nd, and Sm do not contribute to the ferromagnetic order. In the case of *RE* = Pr, this is confirmed by neutron diffraction. In contrast, the magnetic measurements of *RE* = Gd show that the moments of Gd ferromagnetically order with the moments of $[MnSb_4]^{9-}$, and reduced screening of moments on Mn^{2+} is evident. The sensitive variation of magnetic behavior is attributed to the various *RE* substitutions resulting in different interactions of the 4f-orbitals with the 3d-orbitals of Mn in the $[MnSb_4]^{9-}$ cluster conducted through 5p-orbitals of Sb.

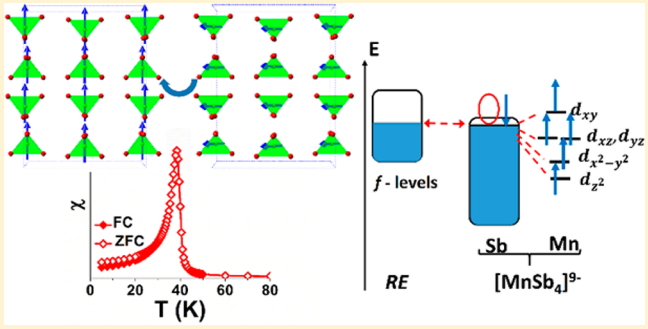

INTRODUCTION

The study of magnetism and magnetic materials such as 3d−4f interaction and single-molecule magnets has been motivating research in chemistry, physics, and materials science.[1,2] Recently, with the discovery of heterometallic complexes containing both transition metals and rare earth elements in single-molecule magnets, 3d−4f interaction has attracted intensive research interest.[3,4] 3d−4f interactions were first studied in intermetallic compounds, and these compounds have complex physical properties such as itinerant magnetism, heavy fermion behavior, and superconductivity. For example, $EuCo_2As_2$ shows itinerant magnetism, and $CeCoIn_5$ is a heavy fermion superconductor with itinerant magnetism.[5−9] Material applications, such as permanent strong magnets, magnetoresistance, and magnetocaloric effects, were also discovered and studied in 3d−4f intermetallic compounds.[10−12]

Named after Eduard Zintl, *Zintl* phases are salt-like intermetallic compounds in which electrons can be considered as completely transferred from cations to anions.[13] The anions or anionic networks in these compounds usually follow valence rules to have stable electronic configurations. When *Zintl* phases were first systematically studied, the component elements were alkali or alkaline earth elements and group IIIA−VA elements.[14] These compounds are diamagnetic or exhibit weak paramagnetism due to the lack of magnetic ions and precise valence. Later the component elements were

Received: June 2, 2016
Published: August 24, 2016

DOI: 10.1021/jacs.6b05636
J. Am. Chem. Soc. 2016, 138, 12422−12431

expanded to include transition metals and rare earth elements, and compounds such as $Yb_{14}MnSb_{11}$, Pr_4MnSb_9, $Ca_{21}Mn_4Sb_{18}$, $Eu_{10}Mn_6Sb_{13}$, $Yb_9Zn_{4+x}Bi_9$, and $Cs_{13}Nb_2In_6As_{10}$ have been synthesized and studied.[15−20] The Mn-containing compounds usually show magnetic order, which opens the study of magnetism in *Zintl* phases and provides avenues to 3d−4f interactions.

Among the compounds mentioned above, $Yb_{14}MnSb_{11}$ (Figure 1) has unique magnetic properties. It crystallizes in

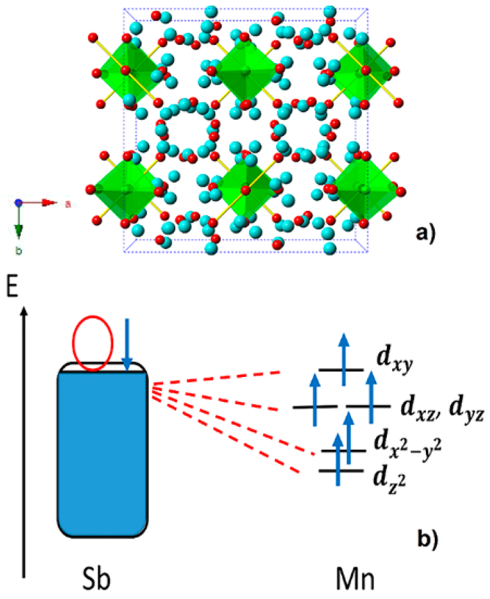

Figure 1. (a) Unit cell of $Yb_{14}MnSb_{11}$ projected along the *c* direction. Blue spheres represent Yb atoms, green tetrahedral represent $[MnSb_4]^{9-}$ cluster, and red spheres represent Sb atoms. (b) Diagram of the (d^5 + *h*) scenario for the $MnSb_4$ tetrahedron in $Yb_{14}MnSb_{11}$.

the $Ca_{14}AlSb_{11}$ structure type with the space group of $I4_1/acd$.[15,21] Each formula unit contains 14 Yb^{2+} cations, one $[MnSb_4]^{9-}$ tetrahedral cluster, one linear Sb_3^{7-} anion, and four isolated Sb^{3-} anions. $Yb_{14}MnSb_{11}$ has a ferromagnetic transition at 53 K, a saturation magnetic moment of 4.2 μ_B at 5 K, and an effective magnetic moment of 4.9 μ_B. In $Yb_{14}MnSb_{11}$, Yb^{2+} is nonmagnetic, and therefore the ferromagnetic transition is due to the order of moments on Mn. The large Mn−Mn distance (~10 Å) indicates that the magnetic ordering is via Ruderman−Kittel−Kasuya−Yosida (RKKY) coupling, which is conducted through carriers.[15,22] X-ray magnetic circular dichroism (XMCD) shows that the $[MnSb_4]^{9-}$ cluster has an electronic state of d^5 + *h* (hole), schematically shown in Figure 1. A hole on Sb, aligned with the d spins on Mn^{2+}, polarizes a spin on the Sb in the $[MnSb_4]^{9-}$ cluster which screens one d electron leading to the description of d^5 + *h*.[23] Calculations of the band structures of iso-structural analogues support this result and indicate that the magnetic unit of $Yb_{14}MnSb_{11}$ is the tetrahedral cluster $[MnSb_4]^{9-}$.[24] Previous studies have shown that chemical substitutions and the structure of the tetrahedral cluster, such as bond lengths and bond angles, affect physical properties such as thermoelectric properties.[25,26] When Yb sites are substituted by other rare earth elements, different magnetic behavior is observed. Below the ferromagnetic ordering temperature, the saturation moment for $Yb_{14-x}RE_xMnSb_{11}$ (*RE* = La and Ce, 0 < *x* < 0.7) is the same as $Yb_{14}MnSb_{11}$ while in $Yb_{14-x}RE_xMnSb_{11}$ (*RE* = Tb, Dy, Ho, and Er, 0 < *x* < 0.5) it increases with *RE* amounts.[22,27−29] This indicates that Ce is not ordered while Tb, Ho, and Er are ferromagnetically ordered with Mn moments. Similar alteration of the magnetic properties by *RE* substitutions has also been observed in $La_{1-x}RE_xCo_2P_2$ (*RE* = Ce, Pr, Nd, and Sm).[30,31] In the case of $Yb_{14-x}RE_xMnSb_{11}$, there is additional complexity associated with site specific substitution for the 4 Yb crystallographic sites related to the size of RE^{3+} ions and the volumes of Yb sites.[32]

In this paper, we systematically study the magnetism of $Yb_{14-x}RE_xMnSb_{11}$ (0 < *x* < 0.6, *RE* = Pr, Nd, Sm, and Gd) to better clarify the 3d−4f interactions in $Yb_{14-x}RE_xMnSb_{11}$ and to contrast the different effects on magnetic properties between trivalent light and heavy rare earth substitutions. A distinct difference in the magnetic order of *RE* substitutions was found between trivalent light and heavy rare earth elements, and a spin reorientation was also discovered. The various magnetic behavior caused by different rare earth substitutions indicates that the Yb/*RE* sublattice and their f-orbitals affect the magnetic properties, although Yb has no magnetic moment in $Yb_{14}MnSb_{11}$.

EXPERIMENTAL SECTION

Reagents. Elemental Yb (Metall Rare Earth Limited, 99.99%), Pr (Ames Lab, 99.99%), Nd (Ames Lab, 99.99%), Sm (Ames Lab, 99.99%), Gd (Ames Lab, 99.99%), Mn (Alfa Aesar, 99.95%), Sb (Alfa Aesar, 99.999%), and Sn (Alfa Aesar, 99.3%) were used for the synthesis of the crystals. Yb, Pr, Nd, Sm, and Gd were cut into small pieces while Mn, Sb, and Sn were used as received. All elements were handled using inert atmosphere techniques, including an argon-filled glovebox with water levels <0.5 ppm.

Synthesis of Single Crystals. Crystals were synthesized by a Sn-flux method.[33,34] The elements were loaded into an alumina crucible by layers, and the ratio of these elements is Yb:Pr/Nd/Sm/Gd:Mn:Sb:Sn = 14 − *p*:*p*:6:11:86, with *p* = 0.1, 0.3, 0.5, 0.7, 0.9, and 1.2 (*p* is the preparative amount of rare earth elements used in the synthesis). Details of flux synthesis has been described in previous papers.[22,35] The high-quality crystals were harvested in an argon-filled glovebox equipped with a microscope. The stoichiometry of resulting crystals was determined from electron microprobe.

Electron Microprobe Analysis. Crystals from magnetization measurement were analyzed using a Cameca SX-100 electron probe microanalyzer equipped with a wavelength-dispersive spectrometer with 20 keV accelerating potential and 20 nA beam current. The samples were mounted in epoxy and polished to a smooth surface. The epoxy and sample were coated with carbon for better conduction. X-ray elemental maps were taken at a representative area for each sample. Net elemental intensities for Yb, Mn, and Sb were determined using wavelength-dispersive spectrum with respect to crystals of $Yb_{14}MnSb_{11}$, and $PrPO_4$, $NdPO_4$, $SmPO_4$, and $GdPO_4$ were respectively used as standards for net elemental intensities of Pr, Nd, Sm, and Gd. The composition of each sample was determined by calculating averages and standard deviations from at least 10 randomly selected data points of the main phase. Backscattered images and analysis are provided in the Supporting Information (SI).

Powder X-ray Diffraction. Powder X-ray diffraction (PXRD) data were collected on a few crystals of each sample, crushed into powder to verify phase purity. Samples were examined using a Bruker zero background holder on a Bruker D8 Advance Diffractometer operated at 40 kV and 40 mA utilizing Cu Kα radiation. Kβ radiation is removed by a Ni filter. The powder diffraction patterns are provided in the SI. WinPLOTR (version Jan 2012) software was used for background subtraction and pattern analysis, and EDPCR 2.00 software was used to perform refinement.[36,37]

Magnetization Measurements. Direct current (DC) magnetization data were measured in a Quantum Design Magnetic Property Measurement System (MPMS) with a superconducting quantum interference device (SQUID) detector. Crystals of ~10 mg were

DOI: 10.1021/jacs.6b05636
J. Am. Chem. Soc. 2016, 138, 12422−12431

individually mounted on a Mylar strip, adhered to Kapton tape, and then inserted into a commercial drinking straw. A negligible background signal from the sample holder can be achieved using this mounting method. Therefore, the data were not corrected for magnetic contributions of the sample holder. Temperature-dependent magnetization was first measured as zero-field-cooled (ZFC) magnetization from T = 5 to 300 K, then back to T = 5 K to get field-cooled (FC) magnetization with an applied field of 100 Oe (FC). Field-dependent magnetization data were measured from H = 0 T up to at least H = 5 T at T = 5 K with the same alignment of crystals. Saturation moments are determined using the values at H = 5 T instead of extracting back to H = 0 because some samples were not fully saturated at the highest field for these measurements.

Alternating current (AC) magnetization data were measured in a Quantum Design Physical Property Measurement System (PPMS). Crystals were measured under an oscillating ac field (H = 0.001 T) and AC frequencies ranging from 10 to 10 000 Hz. The data were collected between 10 and 150 K. Both DC and AC magnetization data were calculated and presented per formula unit.

Neutron Diffraction. Large single crystals of $Yb_{14}MnSb_{11}$, $Yb_{13.72}Pr_{0.28}MnSb_{11}$, and $Yb_{13.47}Pr_{0.53}MnSb_{11}$ (5 mm × 3 mm × 3 mm) were studied by neutron diffraction at HB-3A four-circle single-crystal diffractometer at High Flux Isotope Reactor (HFIR) at Oak Ridge National Laboratory (ORNL). Data were collected with neutron wavelength 1.5424 Å generated from a bent perfect Si-220 monochromator.[38] Data were collected on all samples at 5 K with another data collection on $Yb_{13.47}Pr_{0.53}MnSb_{11}$ at 35 K. The intensities of several selected diffractions were monitored as the temperature increased from 4 to 60 K to observe the magnetic ordering temperature. The nuclear and magnetic structure refinements were carried out using FullProf software.[36]

RESULTS AND DISCUSSION

1. Synthesis, Composition and Structure. Well-formed single crystals were prepared from Sn flux. Backscattered electron images show that these crystals were homogeneous with negligible amount of Sn. (Supporting Information, SI). The amounts of *RE* (Pr, Nd, Sm, and Gd) substitution in the products are determined by wavelength dispersive spectrum (SI). Generally, higher *RE* (Pr, Nd, Sm, and Gd) amounts used in the flux results in higher *RE* (Pr, Nd, Sm, and Gd) content; however, the maximum amount of *RE* (Pr, Nd, Sm, and Gd) substitution in $Yb_{14-x}RE_xMnSb_{11}$ is limited to $x \approx 0.6$, consistent with previous studies of other rare earth elements-substituted samples.[22,27−29] In the text below, the single-crystal samples will be referred to according to the experimentally determined content, x.

PXRD patterns indicated that all samples are of the $Ca_{14}AlSb_{11}$ structure type ($I4_1/acd$) and were refined to obtain lattice parameters.[15] Figure 2 shows a plot of unit cell volumes and c/a ratio as a function of composition, x and *RE*. The unit cell parameters increase with the amount of *RE* substitutions, x, and for the same value of x, decrease with decreasing *RE* radii, consistent with previous studies.[32,39] c/a values are consistent across the series, but Sm and Gd containing compounds are slightly larger at the highest amount of substitution. This may be attributed to different Yb-site preferences of these elements in the structure.[39]

2. $Yb_{14-x}Pr_xMnSb_{11}$. *DC Magnetization Measurements.* Temperature-dependent DC magnetic susceptibility of $Yb_{14-x}Pr_xMnSb_{11}$ (x = 0.08, 0.19, 0.28, 0.32, 0.44, 0.53) crystals show ferromagnetic transitions at ∼39−50 K. Figure 3 shows the temperature-dependent magnetic susceptibility of the lowest and highest studied composition (x = 0.08 and 0.53). The temperature-dependent magnetic susceptibility values of the other compositions are provided in the SI. Similar to

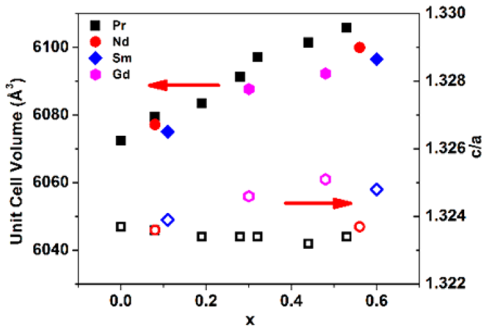

Figure 2. Unit cell volumes and c/a values of $Yb_{14-x}RE_xMnSb_{11}$ (*RE* = Pr, Nd, Sm, and Gd, 0 < x < 0.6). Filled symbols are for unit cell volumes, and hollow symbols are for c/a.

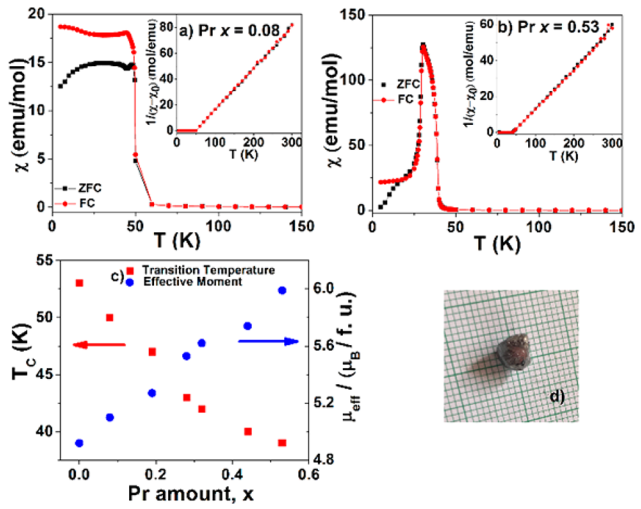

Figure 3. Temperature-dependent susceptibility, FC and ZFC curves of (a) $Yb_{13.92}Pr_{0.08}MnSb_{11}$ and (b) $Yb_{13.47}Pr_{0.53}MnSb_{11}$ with magnetic field of 100 Oe. Inverse susceptibility vs temperature is plotted in the top right. (c) Transition temperature (K) and effective moment (μ_B) vs Pr amount, x. (d) A picture of a typical crystal on 1 mm grid.

$Yb_{14}MnSb_{11}$, which orders ferromagnetically at 53 K, these compositions also show ferromagnetic ordering, but at lower temperatures compared to $Yb_{14}MnSb_{11}$. The Curie temperatures T_C, which are determined from the derivatives of temperature-dependent magnetic susceptibility ($d\chi/dT$), decrease systematically with Pr amount. In the paramagnetic phase, the magnetic susceptibility can be fitted by a Curie−Weiss law (eq 1) using data between 100 and 300 K:

$$\chi = \chi_0 + \frac{C}{T - \theta} \quad (1)$$

where C is the Curie constant, θ is the paramagnetic Weiss temperature, and χ_0 is the temperature-independent paramagnetic term. The results are listed in Table 1. The values of χ_0 for all the samples are small, on the level of 10^{-3} emu/mol, matching with previous results.[22,27] The Curie constants, C, increase with Pr amounts. Effective magnetic moments can be described using eqs 2 and 3:

$$\mu_{eff} = \sqrt{7.99C} \quad (2)$$

$$\mu_{eff}^2 = (1 - x)\mu_{eff}^2(Mn^{2+} + h) + x\mu_{eff}^2(Mn^{2+}) + x\mu_{eff}^2(RE^{3+}) \quad (3)$$

DOI: 10.1021/jacs.6b05636
J. Am. Chem. Soc. 2016, 138, 12422−12431

Table 1. Magnetism Results of $Yb_{14-x}Pr_xMnSb_{11}$ (x = 0.08, 0.19, 0.28, 0.32, 0.44, 0.53)

x	T_C (K)	C (emu·K/mol)[a]	χ_0 (emu/mol)[a]	θ (K)[a]	μ_{eff} (μ_B)[b]	μ_{sat}[5 K] (μ_B)	x_{calc}[c]
0.08	50	3.25(4)	0.0055(2)	46.6(5)	5.10	4.1(2)	0.08
0.19	47	3.48(3)	0.0038(1)	43.1(5)	5.27	4.1(2)	0.16
0.28	43	3.83(7)	0.0091(4)	44.9(7)	5.53	4.2(2)	0.28
0.32	42	3.95(5)	0.0127(3)	43.6(5)	5.62	4.2(2)	0.32
0.44	40	4.12(2)	0.0043(3)	40.5(7)	5.74	4.2(2)	0.38
0.53	39	4.49(5)	0.0061(2)	42.0(4)	5.99	4.5(2)	0.50

[a]From eq 1. [b]From eq 2. [c]From eq 3, employing the ground-state effective moment of Pr^{3+} and the experimental effective moment.

The substitution of $RE = Pr^{3+}$ for Yb^{2+} provides a fraction x of an electron to the formula, filling the hole residing on the orbitals associated with $[MnSb_4]^{9-}$. Thus, Pr^{3+} substitution decreases the carrier concentration, weakens the RKKY interactions, and leads to reduction of the Curie temperature.[21] Filling the hole with x electron also weakens the coupling between spins on Mn and the hole on Sb, and changes the electronic state of Mn from $d^5 + h$ to $[xd^5 + (1 - x)(d^5 + h)]$. The composition of RE, x, determined by microprobe, can be verified by employing the ground-state effective moment of Pr^{3+} estimated from Hund's rule (3.58 μ_B) and the effective moments of Mn $d^5 + h$ ($L = 0$, $S = 2$, μ_{eff} ($Mn^{2+} + h$) = 4.9 μ_B) and d^5 ($L = 0$, $S = 5/2$, μ_{eff} (Mn^{2+}) = 5.9 μ_B).[40] The Pr amount calculated using eq 3 is provided in Table 1 as x_{calc}. The good agreement between calculated and experimental Pr amounts validates eq 3 and supports the idea that the electron provided by Pr^{3+} results in reducing shielding of Mn d^5 spins in the paramagnetic state.

Below the Curie temperatures, $Yb_{14-x}Pr_xMnSb_{11}$ show a bifurcation between zero-field-cooling (ZFC) and field-cooling (FC) curves. This bifurcation is caused by the domain structures and large anisotropy of crystals, having moments of $[MnSb_4]^{9-}$ align along the easy axis (c-axis).[35] Under the condition of ZFC, magnetic moments which are initially antiparallel aligned in adjacent domains at low temperature gradually change from antiparallel to parallel as temperature increases and domains combine. Under the condition of FC, domains are restrained, and magnetic moments tend to be parallel aligned. When temperature is decreased, the susceptibility increases as thermal disruption of moments is depressed.[41] Spin-glass or superparamagnetic behavior can also lead to bifurcations between ZFC and FC curves; therefore, AC susceptibility was also measured for a few samples (SI). No frequency dependence was observed in the curves of χ'. In the curves of χ'', some frequency dependence was observed in the high substitution samples. This has been observed in some typical ordered magnets and attributed to the domain effects related to the large anisotropy.[42,43] Both previous papers and the fact that these samples are homogeneous bulk crystals can also rule out the superparamagnetic scenario.[44,45] The anomaly in ZFC curves for low Pr content x = 0.08 and 0.19 crystals just below T_C has been observed in $Yb_{14}MnSb_{11}$.[24,46] For the high Pr content, x = 0.44 and 0.53 crystals, a sharp drop in magnetic susceptibility is observed at ~30 K in both FC and ZFC curves. This dramatic drop does not resemble an antiferromagnetic transition. Also the positive θ values do not support the identification of this transition as an antiferromagnetic transition. In order to study this magnetic transition, single crystal neutron diffraction was performed, and the results are presented below.

Field-dependent magnetization (Figure 4) shows that samples of x = 0.08–0.44 have similar saturation magnetic moments, ~ 4.1–4.2 μ_B. The values closely match pristine $Yb_{14}MnSb_{11}$, indicating that moments on Pr are not ordered in the ferromagnetic phase since the saturation moment is unaffected by the amount of Pr.[22] This is consistent with neutron diffraction described below. The sample of x = 0.53 has a larger saturation moment, ~ 4.5 μ_B, but the increase is too small to be considered as the possible order of Pr moments. This change may be caused by the crystal field splitting effect of Pr or the unscreening of moments on $[MnSb_4]^{9-}$ when the amount of Pr^{3+} exceeds a critical value. $Yb_{14}MnSb_{11}$ is considered a Kondo lattice compound, and the additional electrons provided to the $[MnSb_4]^{9-}$ cluster may inhibit the screening of Mn moments.[29,47]

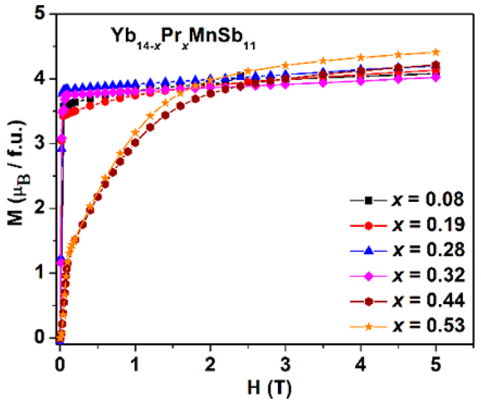

Figure 4. Field-dependent magnetization curves of $Yb_{14-x}Pr_xMnSb_{11}$ (x = 0.08, 0.19, 0.28, 0.32, 0.44, 0.53) at 5K.

Neutron Diffraction. Large crystals of $Yb_{14-x}Pr_xMnSb_{11}$ (x = 0, 0.28, 0.53) were measured by single crystal neutron diffraction. Peak intensities of the (004) and (400) diffractions were scanned with decreasing temperature (Figure 5). When the magnetic moment is parallel to the scattering vector, no magnetic contribution can be seen in the diffraction intensity of corresponding diffractions.[48] For x = 0 and 0.28, the (004) diffraction intensities show no change over temperature while the (400) diffraction intensities start to increase at 52 and 44 K, which are caused by the ferromagnetic transition and consistent with the DC magnetization measurement. For x = 0.53, the (400) diffraction intensity has a similar behavior and the transition temperature, 39 K, matches with magnetization measurement. However, an abnormal peak between 40 and 30 K shows up in the (004) diffraction intensity. This peak is caused by a spontaneous reorientation of magnetic moment driven by temperature. Combined with the refinement on neutron diffraction data, magnetic moments in the samples of x = 0 and 0.28 are parallel to c-direction, consistent with previous conclusions.[15,34] The magnetic moment in the sample of x = 0.53 first aligns in the diagonal of ab-plane and then reorients to the c direction. These results provide a rationale for the

DOI: 10.1021/jacs.6b05636
J. Am. Chem. Soc. 2016, 138, 12422–12431

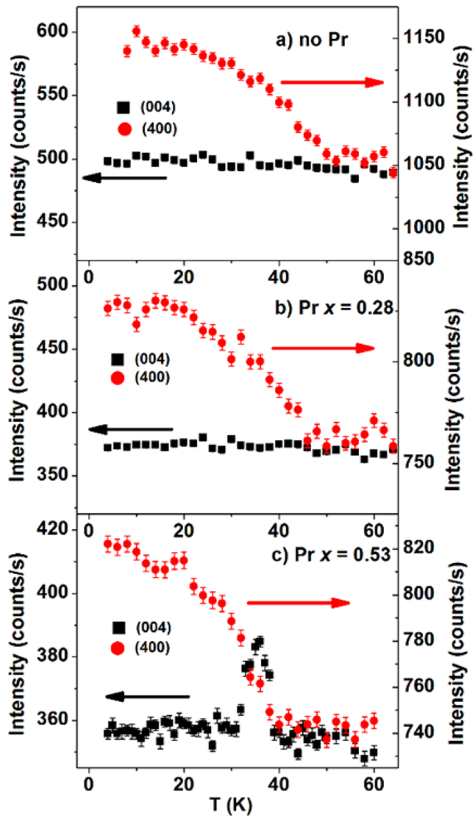

Figure 5. Neutron diffraction intensities of the (004) and (400) of (a) $Yb_{14}MnSb_{11}$, (b) $Yb_{13.72}Pr_{0.28}MnSb_{11}$, and (c) $Yb_{13.47}Pr_{0.53}MnSb_{11}$ scanned over temperature.

unexpected peak in the ZFC and FC curves of $Yb_{13.47}Pr_{0.53}MnSb_{11}$. During the DC magnetization measurement, the crystal of $Yb_{13.47}Pr_{0.53}MnSb_{11}$ is aligned as *ab*-plane is almost parallel to magnetic field. The sharp drop of susceptibility is due to the reorientation of spins from the *ab*-plane to *c* direction.

At 5 K, refinements on the neutron diffraction data show that Mn in $Yb_{14}MnSb_{11}$, $Yb_{13.72}Pr_{0.28}MnSb_{11}$, and $Yb_{13.47}Pr_{0.53}MnSb_{11}$ has a magnetic moment of 4.3(2) μ_B, 4.2(2) μ_B, and 4.3(2) μ_B along the *c*-axis, respectively. There is no observable ordered moment on Pr according to the refinement. The small differences between magnetic moments of Mn given by neutron diffraction and field-dependent magnetization measurement are negligible considering the fact that the complex structure, large unit cell, and only 8 Mn atoms out of 208 atoms in one unit cell lead to small contributions (<10%) of magnetic moments to diffraction intensities. At 35 K, refinement shows that magnetic moments of Mn in $Yb_{13.47}Pr_{0.53}MnSb_{11}$ is 3.0 (2) μ_B, parallel to the [110] direction. Since 35 K is only 4 K lower than the transition temperature of $Yb_{13.47}Pr_{0.53}MnSb_{11}$ (39 K), thermal disruption affects the order of magnetic moments and decreases the measured moments. Field-dependent susceptibility measurement also supports the hypothesis that magnetic moments are not fully ordered at this temperature (SI). The refinement of the structure shows that the unit cell parameters increase with Pr amounts, consistent with the results at room temperature. Among the four Yb sites, Pr prefers Yb(2) sites which form layers between $[MnSb_4]^{9-}$ layers, and this agrees with previous results on $Yb_{14-x}Ce_xMnSb_{11}$ (SI).[22]

Based on the results of neutron diffraction, the temperature-dependent magnetic susceptibility and field-dependent magnetization of an oriented crystal of $Yb_{13.47}Pr_{0.53}MnSb_{11}$ were measured (Figure 6). When the magnetic field is parallel to the [001] direction, the ZFC and FC curves resemble the curves of crystals without spin orientation and show a typical ferromagnetic behavior. Meanwhile, when the magnetic field is parallel to the [100] direction, ZFC and FC curves overlap with each other and have sharp peaks between 30 and 40 K due to the spin reorientation. The overlap of ZFC and FC curves in this case supports previous discussions on the domain structure and anisotropy. When the magnetic field is parallel to the [101] direction, a combination of the [100] and [001] directions can be observed. In the field-dependent measurement at 5 K, the magnetization saturates rapidly when measured along the [001] direction, also indicating that at 5 K the [001] direction is the easy axis. When the magnetic field is parallel to the [100] direction, the magnetic moment linearly increase and almost saturates at approximately 1.5 T. This behavior implies that the spin reorientation is spontaneous and not induced by the magnetic field. The anisotropy of $Yb_{14}MnSb_{11}$ has been studied before, and no spin reorientation was observed.[15,34] $Yb_{13.72}Pr_{0.28}MnSb_{11}$ was measured along several directions to check for anisotropy, and it was found to have a similar behavior to $Yb_{14}MnSb_{11}$ with no spin reorientation.

In summary, the substitution of Pr^{3+} for Yb^{2+} reduces the screening of the Mn moment by filling the hole (by *x* amount) associated with $[MnSb_4]^{9-}$, and thereby decreases the carrier concentration and lowers T_C. When the amount of Pr reaches a critical value ($x \approx 0.44$), a spin reorientation of $[MnSb_4]^{9-}$ moments from *ab*-plane to *c*-axis appears below the Curie temperature along with an increase of saturation moment of $Yb_{13.47}Pr_{0.53}MnSb_{11}$ at 5 K. Previous studies in cyano-bridged salts, MnBi, $RE_2Fe_{14}B$, and $REMO_3$, show that the crystalline electric field (CEF) and the resulting large anisotropy are essential causes of the spin reorientation.[1,49−58] In $RE_2Fe_{14}B$ compounds, two kinds of spin reorientation were discovered: one is a sharp shift of spins and first-order phase transition, while the other is a slow tilt of spins within a temperature region and a second-order phase transition.[52−55] The spin reorientation in $RE_2Fe_{14}B$ is due to the anisotropy of Fe sublattice and *RE* sublattice caused by the combinations of CEF and the exchange field.[54,55] This is similar to rare earth containing oxides, $REMO_3$ (M = Cr, Mn, Fe), although *RE* sublattice has no ordered moments.[56−58] In $Yb_{14-x}Pr_xMnSb_{11}$ ($0.44 \leq x \leq 0.53$), the spin reorientation is a second-order phase transition which is consistent with its measured heat capacity data (SI). The ferromagnetic magnetic interactions in $Yb_{14-x}Pr_xMnSb_{11}$ are dominated by 3d-3d interactions of Mn, however, the 3d−4f interactions between *RE* sublattice and Mn sublattice affect the spin reorientation. Pr prefers Yb(2) sites which form layers between $[MnSb_4]^{9-}$ layers (Figure 6); therefore, the substitution of Pr changes the interactions between $[MnSb_4]^{9-}$ layers. The substitution and the change in structure affect the *RE* sublattice, and this change in *RE* sublattice further alters the CEF and the 3d−4f interactions between *RE* sublattice and Mn sublattice, finally leading to a change of the anisotropy energy.[1] When the *RE* amount reaches a critical value, a qualitative change appears in the magnetic property and anisotropy, causing the spin reorientation behavior. A further thought about the f-levels in Yb atoms may provide another perspective to understand the magnetic behavior. The huge difference in properties between

DOI: 10.1021/jacs.6b05636
J. Am. Chem. Soc. 2016, 138, 12422−12431

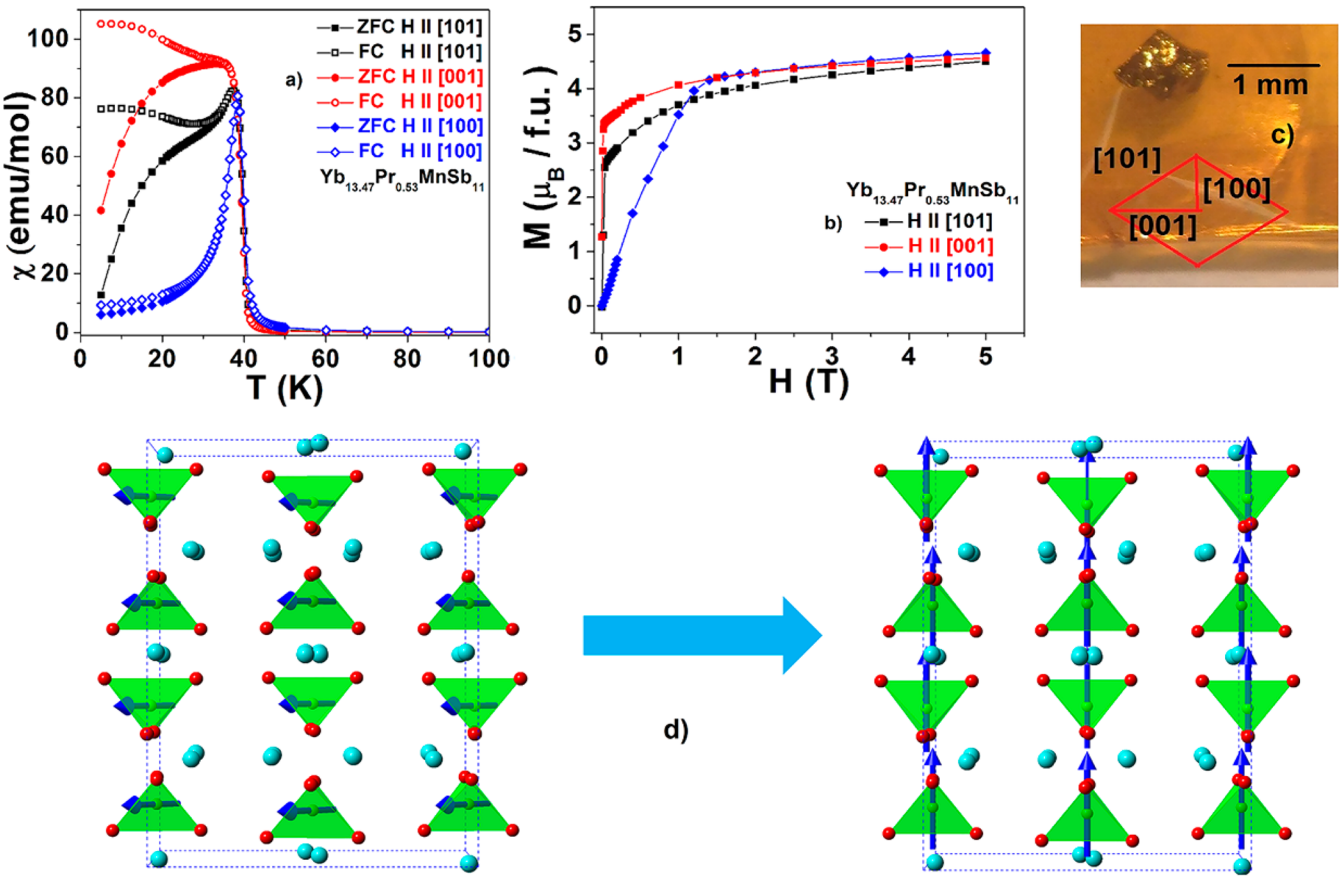

Figure 6. (a) Temperature-dependent magnetic susceptibility of $Yb_{13.47}Pr_{0.53}MnSb_{11}$. FC and ZFC curves along the direction [101], [001], and [100]. (b) Field-dependent magnetization along three directions at 5 K. (c) Picture describing the orientations of the crystal. (d) Plot showing the spin reorientation. The unit cell is projected along *b*-direction. The blue arrows represent spins, green tetrahedral are $[MnSb_4]^{9-}$ cluster, red spheres represent Sb in the $[MnSb_4]^{9-}$ cluster, and light blue spheres represent Yb(2) sites.

$Yb_{14}MnSb_{11}$ and $Ca_{14}MnSb_{11}$ indicates that the f-levels of Yb plays an important role in the physical properties of $Yb_{14}MnSb_{11}$.[15,47,59] The heavy fermion behavior shows that f-levels of Yb make a significant contribution to the band structures near the Fermi-level. When Yb is substituted by Pr, the different f-levels of Pr change the electronic band structure near the Fermi level and lead to a change in magnetic properties, which is similar to previous discussions on carrier concentration and thermoelectric properties.[21]

3. $Yb_{14-x}RE_xMnSb_{11}$ (*RE* = Nd, Sm, and Gd). The magnetic properties of Nd, Sm, and Gd substitutions are discussed in comparison with the Pr-substituted samples. Results of DC temperature-dependent magnetic susceptibility and field-dependent magnetization of $Yb_{14-x}RE_xMnSb_{11}$ (*RE* = Nd, Sm, and Gd) are listed in Figure 7 and Table 2. The substitutions of both Nd and Sm cause reductions in the Curie temperatures. The bifurcation between ZFC and FC curves is also observed in Nd and Sm substitutions, showing a large anisotropy of magnetism. The spin reorientation is observed in $Yb_{13.44}Nd_{0.56}MnSb_{11}$. At the Curie temperature (39 K), Mn moments in $Yb_{13.44}Nd_{0.56}MnSb_{11}$ first order along [110] direction and then reorient to [001] direction at 25 K. The spin reorientation causes FC and ZFC curves to have peaks between 25 and 39 K when the field is parallel to *ab*-plane and an anomaly when the field is parallel to *c*-axis. The anomaly differs from the curves of $Yb_{13.47}Pr_{0.53}MnSb_{11}$, and it may be caused by the wider spin reorientation temperature region of $Yb_{13.44}Nd_{0.56}MnSb_{11}$ (39−25 K). Field-dependent magnetization measurements show that these crystals have saturation moments of ∼4 μ_B, indicating that Nd^{3+} and Sm^{3+} are not magnetically ordered at 5 K. $Yb_{13.44}Nd_{0.56}MnSb_{11}$ has a saturation moment of 3.8 μ_B, smaller than $Yb_{14}MnSb_{11}$. On the contrary, no spin reorientation or change of saturation moment in Sm-substituted samples is noticed. In the paramagnetic phase, eq 3 is a good description of magnetic behavior using the effective moments of Nd^{3+} (3.62 μ_B) and Sm^{3+} (0.84 μ_B) derived from Hund's rules, consistent with *RE* = Pr compounds.[40] Calculations based on eq 3 give substitution amounts matching the experimentally determined values.

Magnetic properties of Gd-substituted samples, $Yb_{13.70}Gd_{0.30}MnSb_{11}$ and $Yb_{13.52}Gd_{0.48}MnSb_{11}$, are different from those of Pr-, Nd-, and Sm-substituted samples in many aspects. ZFC and FC curves of Gd-substituted samples do not show large bifurcations in the ferromagnetic phase, indicating a small anisotropy of magnetism. $Yb_{13.70}Gd_{0.30}MnSb_{11}$ (46 K) and $Yb_{13.52}Gd_{0.48}MnSb_{11}$ (45 K) have almost the same Curie temperatures, which are lower than that of $Yb_{14}MnSb_{11}$ but higher than those of Pr, Nd, and Sm substitutions with the similar amounts. Field-dependent DC magnetization of Gd-substituted samples also show a much larger saturation moments than those of Pr-, Nd-, and Sm-substituted samples at 5 K. The significantly larger values mean the moments on Gd^{3+} order ferromagnetically with the moments on $[MnSb_4]^{9-}$. The effective and saturation moments on Gd^{3+} and $[MnSb_4]^{9-}$ can be calculated by eq 3 provided previously and eq 4:

DOI: 10.1021/jacs.6b05636
J. Am. Chem. Soc. 2016, 138, 12422−12431

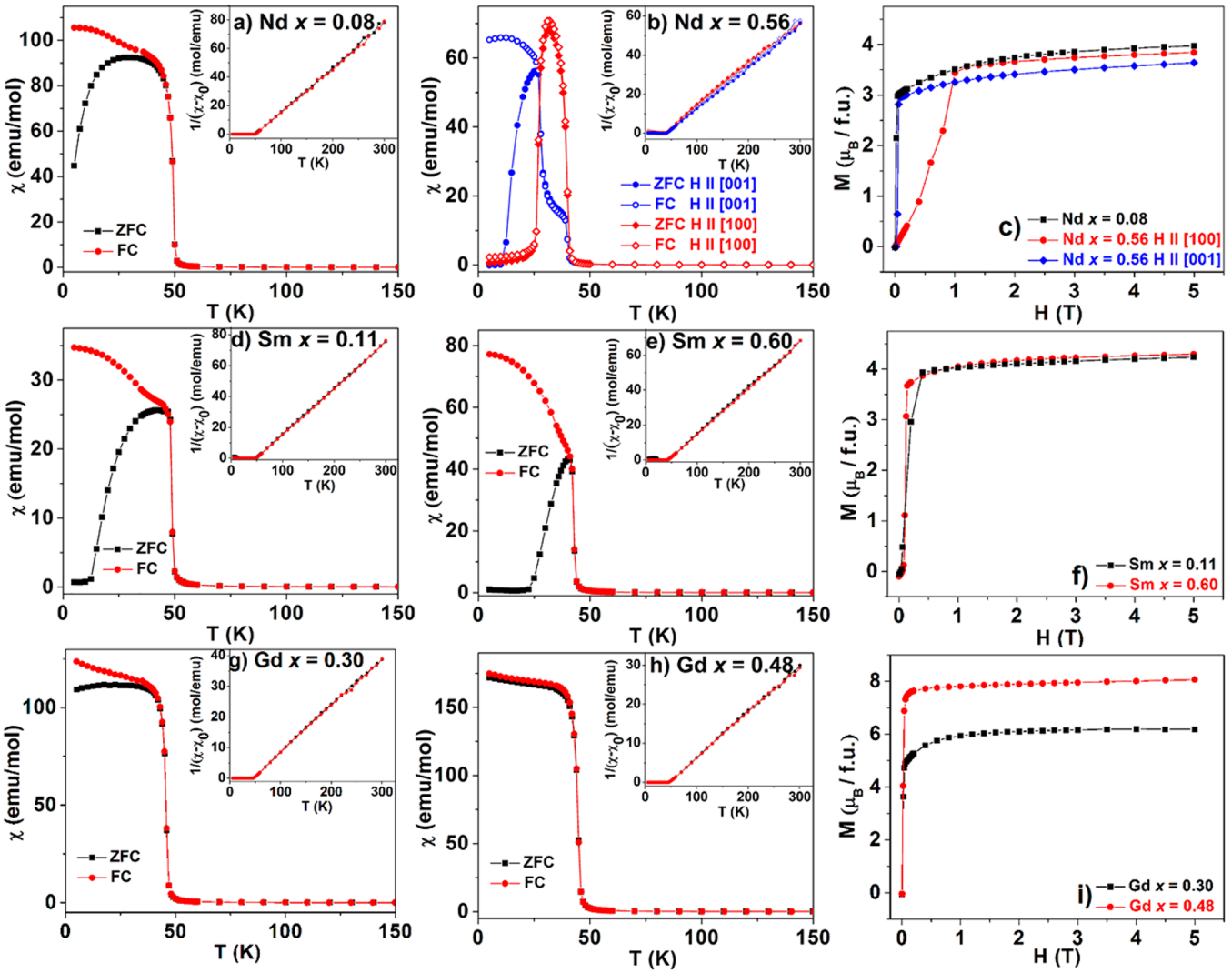

Figure 7. Temperature-dependent magnetic susceptibility of $Yb_{14-x}RE_xMnSb_{11}$ with field of 100 Oe: (a) *RE* = Nd and $x = 0.08$, (b) *RE* = Nd and $x = 0.56$, (d) *RE* = Sm and $x = 0.11$, (e) *RE* = Sm and $x = 0.60$, (g) *RE* = Gd and $x = 0.30$, and (h) *RE* = Gd and $x = 0.48$. Also shown are their field-dependent magnetization curves at 5 K: (c) *RE* = Nd, (f) *RE* = Sm, and (i) *RE* = Gd.

Table 2. Magnetism Results of $Yb_{14-x}RE_xMnSb_{11}$ (*RE* = Nd, Sm, and Gd)

x	T_C (K)	C (emu·K/mol)[a]	χ_0 (emu/mol)[a]	θ (K)[a]	μ_{eff} (μ_B)[b]	μ_{sat}[5 K] (μ_B)	x_{calc}[c]
			RE = Nd				
0.08	49	3.23(3)	0.0069(2)	50.0(3)	5.08	4.0(2)	0.07
0.56	40	4.68(7)	0.0044(3)	39.8(6)	6.11	3.8(2)	0.56
			RE = Sm				
0.11	49	3.16(1)	0.0070(1)	49.3(1)	5.02	4.2(2)	0.11
0.60	42	3.86(3)	0.0015(1)	45.7(2)	5.55	4.2(2)	0.58
			RE = Gd				
0.30	46	6.37(3)	0.0041(3)	48.7(1)	7.13	6.9(2)	0.36
0.48	45	7.53(3)	0.0025(2)	49.6(1)	7.76	8.1(2)	0.48

[a]From eq 1. [b]From eq 2. [c]From eq 3, employing the corresponding ground-state effective moments and the experimental effective moment.

$$\mu_{sat} = (1 - x)\mu_{sat}(Mn^{2+} + h) + x\mu_{sat}(Mn^{2+}) + x\mu_{sat}(Gd^{3+}) \quad (4)$$

Using the Gd^{3+} moments from Hund's rules (7.94 μ_B for effective moment and 7 μ_B for saturation moment), the calculated amounts of Gd (x_{calc}) are consistent with the results of experimental values for both effective and saturation moments.[40] Therefore, similar to Pr, Nd, and Sm, in the paramagnetic phase the electron donated by Gd fills the hole in the $[MnSb_4]^{9-}$ tetrahedral cluster and unscreens the 3d electrons so that the total effective moment is described by eq 3. Different from Pr, Nd, and Sm, in the ferromagnetic phase the local saturation moment is best described by eq 4, where Gd^{3+} moments ferromagnetically couple with the moments of $[MnSb_4]^{9-}$ cluster. Similar phenomenon has been observed in

DOI: 10.1021/jacs.6b05636
J. Am. Chem. Soc. 2016, 138, 12422−12431

$Eu_{14}MnSb_{11}$. The ferromagnetic ordering temperature is increased to ~100 K, and the spin-only Eu^{2+} moments order ferromagnetically with those of $[MnSb_4]^{9-}$ cluster.[60]

Comparing all the substitutions, similar maximum of substitutions (~0.5−0.6) show that the structure of $Yb_{14}MnSb_{11}$ has intrinsic electronic consistency. This consistency limits the maximum of substitution and cannot be easily altered by substitutions. However, a clear change in magnetism appears when f-orbitals of substitutions change from less than half-filled to half-filled or more than half-filled. Curie temperatures as a function to *RE* in $Yb_{14-x}RE_xMnSb_{11}$ with x reaching the maximum for each rare earth substitution is shown in Figure 8. The Curie temperature (T_C) first increases from La

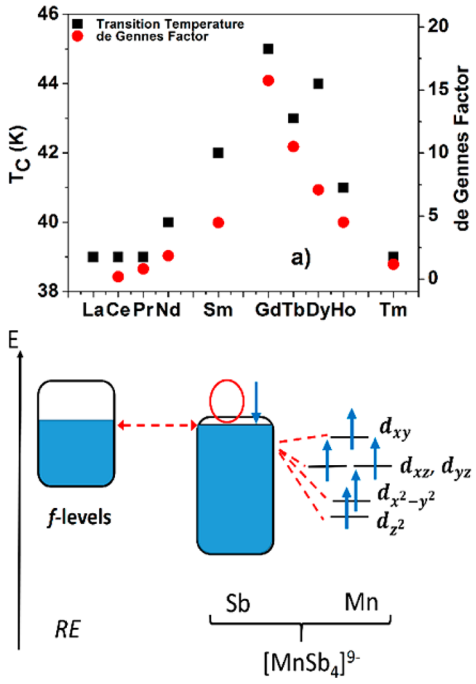

Figure 8. (a) Curie temperature and de Gennes factors (dG = $(g-1)^2J(J+1)$) vs *RE* in $Yb_{14-x}RE_xMnSb_{11}$ ($x \approx 0.5$, is the maximum for each *RE*). (b) Diagram of the 3d−4f interactions scenario for $Yb_{14-x}RE_xMnSb_{11}$.

(39 K) to Gd (45 K) and then decreases until T_m (39 K), with Gd substitution having the highest T_C. The Curie temperatures are theoretically expected to be the same with the same amount of trivalent *RE* substitutions based on RKKY theory, since in principle all *RE* contribute ~0.5 e^- to the compound, reducing the carrier concentration in an identical fashion. However, the correspondence of Curie temperatures to the de Gennes factors ($(g-1)^2J(J+1)$) of trivalent *RE* substitutions indicates that f-levels of *RE* substitutions interact with the bands near Fermi level, have an effect on the Mn sublattice, and change the 3d−4f interactions, which is important in magnetic exchange interactions in addition to carrier concentration.

When Yb is substituted by light rare earth elements (*RE* = La, Ce, Pr, Nd, and Sm), the largest difference is the appearance of spin reorientation in Pr- and Nd-substituted samples. Moments on light *RE* elements are not ordered since the saturation moments (~4 μ_B) of crystals are not linearly related to the *RE* content, x. However, small changes of saturation moments are observed in Pr- and Nd-substituted samples at the highest x. The similarities in light rare earth substitutions exclude simple explanations for spin reorientation such as carrier concentration and site preference. Another fact supporting this explanation is that $Yb_{14}MnBi_{11}$ has spin reorientation behavior.[15] Compared with $Yb_{14}MnSb_{11}$, $Yb_{14}MnBi_{11}$ is more metallic with higher carrier concentration. Therefore, this spin reorientation is caused by the complex electronic interactions and change of anisotropy caused by different *RE* substitutions.

Mn are unscreened by the corresponding fraction of electron (x) in $Yb_{14-x}Gd_xMnSb_{11}$, and the local moment of Gd^{3+} orders ferromagnetically with the Mn moments. Another difference is that Gd-substituted samples have a much smaller anisotropy, a result of the half-filled f-orbitals with no orbital contributions to magnetic moments. Since magnetic moments on Mn^{2+} (5 μ_B) also have no orbital contributions, Gd substitutions reveals the spin-only interactions in the system.

Previous magnetic studies on $Yb_{14-x}RE_xMnSb_{11}$ (*RE* = Tb, Dy, Ho, and Tm) show similar behavior in the paramagnetic phase but different results in the ferromagnetic phase.[27,28] Above the Curie temperature, the effective moments are contributed by local moments and can be described using eq 3. Below the Curie temperature, the moments on *RE* (*RE* = Tb, Dy, Ho, and Tm) substitutions are ferromagnetically ordered with $[MnSb_4]^{9-}$ but only a fraction of the theoretical moments were observed, which cannot be described using simple mathematical equations.

In summary, all *RE* substitutions can be classified into three categories based on the interactions between their moments and the moments of $[MnSb_4]^{9-}$ in the ferromagnetic phase. Generally speaking, when the 4f-orbital of RE^{3+} is less than half-filled, their moments are not ordered, while half-filled or more than half-filled 4f-orbitals lead to ferromagnetic order of moments on RE^{3+} with spin-only Gd^{3+} as a special case.

To further understand and clarify the 3d−4f interactions in $Yb_{14-x}RE_xMnSb_{11}$, an explanation is proposed based on the previous spin polarization calculations on $Ca/Ba_{14}MnBi_{11}$ employing a local orbital-based method within the local spin-density approximation, site preferences of *RE* atoms in $Yb_{14}MnSb_{11}$ and previous theories of Fe-*RE* compounds.[24,32,61,62] The hole on Sb in the $[MnSb_4]^{9-}$ cluster polarizes a spin (considered as downward) which is antiparallel to the spins on Mn (considered as upward). Meanwhile, this spin mainly interacts with and polarizes adjacent Yb/*RE* atoms, which are the Yb(1) and Yb(3) sites in the structure.[24] Considering the fact that light *RE*s prefer Yb(2) and Yb(4) sites, the magnetic results are consistent with the non-order of moments on light *RE* substitutions.[32] For the heavy *RE* substitutions, which prefer Yb(1) and Yb(3) sites, 5d-orbitals on *RE* may hybridize with 5p-orbitals on Sb. Previous studies on Fe-*RE* have shown that this hybridization leads to antiparallel spins on related atoms.[61−64] As the spin on Sb is downward, spins on the *RE* should be upward, parallel to spins on Mn. Since spins and orbitals have the same direction in heavy *RE*, moments on *RE* are ferromagnetically coupled with moments on Mn. Gd substitution shows the spin-only condition. For other heavy *RE* substitutions, the scenario is more complex, involving orbital contributions and crystal field splitting effects.[1] The 3d−4f interactions in $Yb_{14-x}RE_xMnSb_{11}$ are different from the 3d−4f interactions of Fe-*RE* compounds in that the spins in 3d-orbitals of Fe and 4f-orbitals of *RE* are antiparallel.[63,64] The difference may be explained using the fact that the interaction between Mn and *RE* is conducted through

DOI: 10.1021/jacs.6b05636
J. Am. Chem. Soc. 2016, 138, 12422−12431

the hole and the polarized spin on Sb, which has an antiparallel direction to the spins on Mn.

SUMMARY

Crystals of $Yb_{14-x}RE_xMnSb_{11}$ (*RE* = Pr, Nd, Sm, and Gd, $0 < x < 0.6$), iso-structural with $Ca_{14}AlSb_{11}$, were synthesized by Sn-flux method. They were characterized by powder X-ray diffraction and electron microprobe to verify compositions. The paramagnetic behavior of Pr-, Nd-, and Sm-substituted samples can be described as the addition of electrons reducing the screening of $[MnSb_4]^{9-}$ cluster moments along with the moments of the corresponding amounts of *RE*. The magnetic behavior below the Curie temperature is different depending on the identity of the RE^{3+} substituents. Spin reorientation behavior, which was attributed to the large anisotropy caused by Pr and Nd substitutions, was demonstrated to be from the *ab*-plane to *c*-axis by single crystal neutron diffraction when Pr and Nd substitution amounts reached a critical value (~0.44). Saturation moments were slightly changed by high contents of substitution. The lack of Pr^{3+} contribution to the ferromagnetic order was confirmed by neutron diffraction. The spin reorientation and change of saturation moments are absent in Sm-substituted samples. Gd differs from the lighter *RE* substitutions in that Gd is ferromagnetically ordered with the moments on $[MnSb_4]^{9-}$ and that reduced screening of $[MnSb_4]^{9-}$ can be observed in the saturation moment. Our investigations have revealed that f-levels of *RE* substitutions are crucial to the magnetic properties, and the 3d−4f magnetic interactions in $Yb_{14-x}RE_xMnSb_{11}$ are proposed to be intermediated by the hole on Sb and adjacent Yb sites. Further theoretical and experimental studies are necessary to better clarify and understand the magnetic interactions in this system and analogues.

ASSOCIATED CONTENT

Supporting Information

The Supporting Information is available free of charge on the ACS Publications website at DOI: 10.1021/jacs.6b05636.

Ratio of elements in synthesis and compositions of crystals for all the samples determined by wavelength dispersive spectrum; backscattered electron image of crystals; PXRD patterns of crystals; unit cell parameters refined from PXRD patterns; temperature-dependent susceptibility of $Yb_{14-x}Pr_xMnSb_{11}$ (x = 0.19, 0.28, 0.32, 0.44) under magnetic field of 100 Oe; ac susceptibility of $Yb_{14}MnSb_{11}$, $Yb_{13.72}Pr_{0.28}MnSb_{11}$, $Yb_{13.47}Pr_{0.53}MnSb_{11}$, $Yb_{13.44}Nd_{0.56}MnSb_{11}$, $Yb_{13.40}Sm_{0.60}MnSb_{11}$; neutron diffraction refinement parameters; field-dependent curve of $Yb_{13.47}Pr_{0.53}MnSb_{11}$ at 38.5 K; refined occupancies of Pr in Yb sites; heat capacity of $Yb_{13.47}Pr_{0.53}MnSb_{11}$ between 2 and 100 K (PDF)

AUTHOR INFORMATION

Corresponding Author

*smkauzlarich@ucdavis.edu

Notes

The authors declare no competing financial interest.

ACKNOWLEDGMENTS

We thank Peter Klavins for help with magnetization measurement, and Nicholas Botto and Greg Baxter for the help in electron microprobe measurements. The work at UC Davis, Rice University, and Institute of Chemistry of Tajik Academy of Sciences were respectively supported by U.S. National Science Foundation (DMR-1405973), Gordon and Betty Moore Foundation's EPiQS (GBMF 4417), and International Science & Technology Center (ISTC Project T-2067). The research at ORNL High Flux Isotope Reactor was supported by the Scientific User Facilities Division, Office of Basic Energy Sciences, U.S. Department of Energy.

REFERENCES

(1) Kuz'min, M. D.; Tishin, A. M. Theory of Crystal-Field Effects in 3d-4f Intermetallic Compounds. In *Handbook of Magnetic Materials*; Elsevier: Amsterdam, The Netherlands, 2015.

(2) Sessoli, R.; Tsai, H. L.; Schake, A. R.; Wang, S.; Vincent, J. B.; Folting, K.; Gatteschi, D.; Christou, G.; Hendrickson, D. N. *J. Am. Chem. Soc.* **1993**, *115*, 1804.

(3) Andruh, M.; Costes, J. P.; Diaz, C.; Gao, S. *Inorg. Chem.* **2009**, *48*, 3342.

(4) Rosado Piquer, L.; Sanudo, E. C. *Dalton Trans.* **2015**, *44*, 8771.

(5) Movshovich, R.; Jaime, M.; Thompson, J. D.; Petrovic, C.; Fisk, Z.; Pagliuso, P. G.; Sarrao, J. L. *Phys. Rev. Lett.* **2001**, *86*, 5152.

(6) Steglich, F.; Aarts, J.; Bredl, C. D.; Lieke, W.; Meschede, D.; Franz, W.; Schäfer, H. *Phys. Rev. Lett.* **1979**, *43*, 1892.

(7) Curro, N. J.; Young, B. L.; Schmalian, J.; Pines, D. *Phys. Rev. B: Condens. Matter Mater. Phys.* **2004**, *70*, 235117.

(8) Nakatsuji, S.; Pines, D.; Fisk, Z. *Phys. Rev. Lett.* **2004**, *92*, 016401.

(9) Tan, X.; Fabbris, G.; Haskel, D.; Yaroslavtsev, A. A.; Cao, H.; Thompson, C. M.; Kovnir, K.; Menushenkov, A. P.; Chernikov, R. V.; Garlea, V. O.; Shatruk, M. *J. Am. Chem. Soc.* **2016**, *138*, 2724.

(10) Herbst, J. F.; Croat, J. J.; Yelon, W. B. *J. Appl. Phys.* **1985**, *57*, 4086.

(11) Kim, S. H.; Seo, D. K.; Kremer, R. K.; Kohler, J.; Villesuzanne, A.; Whangbo, M. H. *Chem. Mater.* **2005**, *17*, 6338.

(12) Shen, B. G.; Sun, J. R.; Hu, F. X.; Zhang, H. W.; Cheng, Z. H. *Adv. Mater.* **2009**, *21*, 4545.

(13) Kauzlarich, S. M. *Chemistry, Structure, and Bonding of Zintl Phases and Ions: Selected Topics and Recent Advances*; Wiley-VCH: Weinheim, Germany, 1996.

(14) Schafer, H.; Eisenmann, B.; Muller, W. *Angew. Chem., Int. Ed. Engl.* **1973**, *12*, 694.

(15) Chan, J. Y.; Olmstead, M. M.; Kauzlarich, S. M.; Webb, D. J. *Chem. Mater.* **1998**, *10*, 3583.

(16) Chen, X.; Shen, J. N.; Wu, L. M.; Chen, L. *Inorg. Chem.* **2013**, *52*, 7441.

(17) Holm, A. P.; Kauzlarich, S. M.; Morton, S. A.; Waddill, G. D.; Pickett, W. E.; Tobin, J. G. *J. Am. Chem. Soc.* **2002**, *124*, 9894.

(18) Holm, A. P.; Park, S. M.; Condron, C. L.; Olmstead, M. M.; Kim, H.; Klavins, P.; Grandjean, F.; Hermann, R. P.; Long, G. J.; Kanatzidis, M. G.; Kauzlarich, S. M.; Kim, S. J. *Inorg. Chem.* **2003**, *42*, 4660−4667.

(19) Xia, S. Q.; Bobev, S. *J. Am. Chem. Soc.* **2007**, *129*, 10011.

(20) Gascoin, F.; Sevov, S. C. *Inorg. Chem.* **2003**, *42*, 8567.

(21) Cordier, G.; Schäfer, H.; Stelter, M. *Z. Anorg. Allg. Chem.* **1984**, *519*, 183.

(22) Grebenkemper, J. H.; Kauzlarich, S. M. *APL Mater.* **2015**, *3*, 041503.

(23) Holm, A. P.; Kauzlarich, S. M.; Morton, S. A.; Waddill, G. D.; Pickett, W. E.; Tobin, J. G. *J. Am. Chem. Soc.* **2002**, *124*, 9894.

(24) Sánchez-Portal, D.; Martin, R. M.; Kauzlarich, S. M.; Pickett, W. E. *Phys. Rev. B: Condens. Matter Mater. Phys.* **2002**, *65*, 144414.

(25) Xu, J.; Kleinke, H. *J. Comput. Chem.* **2008**, *29*, 2134.

(26) Hu, Y.; Wang, J.; Kawamura, A.; Kovnir, K.; Kauzlarich, S. M. *Chem. Mater.* **2015**, *27*, 343.

(27) Roudebush, J. H.; Grebenkemper, J.; Hu, Y.; Kazem, N.; Abdusalyamova, M. N.; Kauzlarich, S. M. *J. Solid State Chem.* **2014**, *211*, 206.

DOI: 10.1021/jacs.6b05636
J. Am. Chem. Soc. 2016, 138, 12422−12431

(28) Grebenkemper, J. H.; Hu, Y.; Abdusalyamova, M. N.; Makhmudov, F. A.; Kauzlarich, S. M. *J. Solid State Chem.* **2016**, *238*, 321.
(29) Sales, B. C.; Khalifah, P.; Enck, T. P.; Nagler, E. J.; Sykora, R. E.; Jin, R.; Mandrus, D. *Phys. Rev. B: Condens. Matter Mater. Phys.* **2005**, *72*, 205207.
(30) Kovnir, K.; Thompson, C. M.; Zhou, H. D.; Wiebe, C. R.; Shatruk, M. *Chem. Mater.* **2010**, *22*, 1704.
(31) Thompson, C. M.; Arico, A. A.; Kovnir, K.; Shatruk, M. *J. Appl. Phys.* **2010**, *107*, 09E316.
(32) Vasilyeva, I. G.; Nikolaev, R. E.; Abdusaljamova, M. N.; Kauzlarich, S. M. *J. Mater. Chem. C* **2016**, *4*, 3342.
(33) Fisher, I. R.; Shapiro, M. C.; Analytis, J. G. *Philos. Mag.* **2012**, *92*, 2401.
(34) Canfield, P. C.; Fisk, Z. *Philos. Mag. B* **1992**, *65*, 1117.
(35) Fisher, I. R.; Wiener, T. A.; Bud'ko, S. L.; Canfield, P. C.; Chan, J. Y.; Kauzlarich, S. M. *Phys. Rev. B: Condens. Matter Mater. Phys.* **1999**, *59*, 13829.
(36) Rodriguez-Carvajal, J.; Roisnel, T. WinPLOTR: A Windows Tool for Powder Diffraction Pattern Analysis. In *Proceedings of the Seventh European Powder Diffraction Conference*, Barcelona, Spain, May 20−23, 2000; Delhez, R., Mittemeijer, E. J., Eds.; Trans Tech Publications: Stafa, Switzerland, 2001; Vols. *378*−*381*, pp 118−123.
(37) Rodríquez-Carvajal, J. *Phys. B* **1993**, *192*, 55.
(38) Chakoumakos, B. C.; Cao, H.; Ye, F.; Stoica, A. D.; Popovici, M.; Sundaram, M.; Zhou, W.; Hicks, J. S.; Lynn, G. W.; Riedel, R. A. *J. Appl. Crystallogr.* **2011**, *44*, 655.
(39) Hu, Y.; Bux, S. K.; Grebenkemper, J. H.; Kauzlarich, S. M. *J. Mater. Chem. C* **2015**, *3*, 10566.
(40) Buschow, K. H. J.; de Boer, F. R. *Physics of Magnetism and Magnetic Materials*; Kluwer Academic /Plenum Publishers: New York, 2003.
(41) Craik, D. J. *Magnetism: principles and Applications*; Wiley: West Sussex, U.K., 1995.
(42) Chen, D. X.; Skumryev, K.; Coey, M. D. *Phys. Rev. B: Condens. Matter Mater. Phys.* **1996**, *53*, 15014.
(43) Tsurkan, V.; Hemberger, J.; Klemm, M.; Klimm, S.; Loidl, A.; Horn, S.; Tidecks, R. *J. Appl. Phys.* **2001**, *90*, 4639.
(44) Mydosh, J. A. *Spin glass: an experimental introduction*; Taylor & Francis: Washington, DC, 1993.
(45) Bedanta, S.; Kleemann, W. *J. Phys. D: Appl. Phys.* **2009**, *42*, 013001.
(46) Srinath, S.; Poddar, P.; Srikanth, H.; Sales, B. C.; Mandrus, D. *Phys. Rev. Lett.* **2005**, *95*, 227205.
(47) Burch, K. S.; Schafgans, A.; Butch, N. P.; Sayles, T. A.; Maple, M. B.; Sales, B. C.; Mandrus, D.; Basov, D. N. *Phys. Rev. Lett.* **2005**, *95*, 046401.
(48) Rietveld, H. M. *J. Appl. Crystallogr.* **1969**, *2*, 65.
(49) Larionova, J.; Clerac, R.; Sanchiz, J.; Kahn, O.; Golhen, S.; Ouahab, L. *J. Am. Chem. Soc.* **1998**, *120*, 13088.
(50) Larionova, J.; Kahn, O.; Gohlen, S.; Clerac, R.; Ouahab, L.; Sanchiz, J. *J. Am. Chem. Soc.* **1999**, *121*, 3349.
(51) McGuire, M. A.; Cao, H.; Chakoumakos, B. C.; Sales, B. C. *Phys. Rev. B: Condens. Matter Mater. Phys.* **2014**, *90*, 174425.
(52) Davis, R. L.; Day, R. K.; Dunlop, J. B. *Solid State Commun.* **1985**, *56*, 181.
(53) Hirosawa, S.; Sagawa, M. *Solid State Commun.* **1985**, *54*, 335.
(54) Hirosawa, S.; Matsuura, Y.; Yamamoto, H.; Fujimura, S.; Sagawa, M.; Yamauchi, H. *J. Appl. Phys.* **1986**, *59*, 873.
(55) Kou, X. C.; Grossinger, R.; Hilscher, G.; Kirchmayr, H. R.; de Boer, F. R. *Phys. Rev. B: Condens. Matter Mater. Phys.* **1996**, *54*, 6421.
(56) Correia, A. C.; Laskar, J. *Nature* **2004**, *429*, 848.
(57) Daniels, L. M.; Weber, M. C.; Lees, M. R.; Guennou, M.; Kashtiban, R. J.; Sloan, J.; Kreisel, J.; Walton, R. I. *Inorg. Chem.* **2013**, *52*, 12161.
(58) Fabreges, X.; Petit, S.; Mirebeau, I.; Pailhes, S.; Pinsard, L.; Forget, A.; Fernandez-Diaz, M. T.; Porcher, F. *Phys. Rev. Lett.* **2009**, *103*, 067204.
(59) Rehr, A.; Kuromoto, T. Y.; Kauzlarich, S. M.; Del Castillo, J.; Webb, D. J. *Chem. Mater.* **1994**, *6*, 93.
(60) Chan, J. Y.; Wang, M. E.; Rehr, A.; Kauzlarich, S. M.; Webb, D. J. *Chem. Mater.* **1997**, *9*, 2131.
(61) Buschow, K. H. J. *Rep. Prog. Phys.* **1991**, *54*, 1123.
(62) Herbst, J. F. *Rev. Mod. Phys.* **1991**, *63*, 819.
(63) Szpunar, B. *Physica B+C* **1985**, *130*, 29.
(64) Yamada, H. *Physica B+C* **1988**, *149*, 390.

DOI: 10.1021/jacs.6b05636
J. Am. Chem. Soc. 2016, 138, 12422−12431